



Imaging prediction of nonalcoholic steatohepatitis using computed tomography texture analysis

Shotaro Naganawa¹ · Kenichiro Enooku² · Ryosuke Tateishi² · Hiroyuki Akai³ · Koichiro Yasaka³ · Junji Shibahara⁴ · Tetsuo Ushiku⁵ · Osamu Abe¹ · Kuni Ohtomo⁶ · Shigeru Kiryu⁷ 

Received: 29 September 2017 / Revised: 10 December 2017 / Accepted: 20 December 2017 / Published online: 5 February 2018
© European Society of Radiology 2018

Abstract

Objectives To determine if texture analysis of non-contrast-enhanced CT (NECT) images is able to predict nonalcoholic steatohepatitis (NASH).

Methods NECT images from 88 patients who underwent a liver biopsy for the diagnosis of suspected NASH were assessed and texture feature parameters were obtained without and with filtration. The patient population was divided into a predictive learning dataset and a validation dataset, and further divided into groups according to the prediction of liver fibrosis as assessed by hyaluronic acid levels. The reference standard was the histological result of a liver biopsy. A predictive model for NASH was developed using parameters derived from the learning dataset that demonstrated areas under the receiver operating characteristic curve (AUC) of >0.65. The resulting model was then applied to the validation dataset.

Results In patients without suspected fibrosis, the texture parameter mean without filter and skewness with a 2-mm filter were selected for the NASH prediction model. The AUC of the predictive model for the validation dataset was 0.94 and the accuracy was 94%. In patients with suspicion of fibrosis, the mean without filtration and kurtosis with a 4-mm filter were selected for the NASH prediction model. The AUC for the validation dataset was 0.60 and the accuracy was 42%.

Conclusions In patients without suspicion of fibrosis, NECT texture analysis effectively predicted NASH.

Key Points

- In patients without suspicion of fibrosis, NECT texture analysis effectively predicted NASH.
- The mean without filtration and skewness with a 2-mm filter were modest predictors of NASH in patients without suspicion of liver fibrosis.
- Hepatic fibrosis masks the characteristic texture features of NASH.

Keywords Pattern recognition, Automated · Hepatitis · Fatty liver · Computed tomography · Radiomics

Shotaro Naganawa and Shigeru Kiryu contributed equally to this work.

✉ Shigeru Kiryu
kiryu-ty@umin.ac.jp

¹ Department of Radiology, Graduate School of Medicine, The University of Tokyo, 7-3-1, Hongo, Bunkyo-ku, Tokyo 113-0033, Japan

² Department of Gastroenterology, Graduate School of Medicine, The University of Tokyo, 7-3-1, Hongo, Bunkyo-ku, Tokyo 113-0033, Japan

³ Department of Radiology, The Institute of Medical Science, The University of Tokyo, 4-6-1, Shirokanedai, Minato-ku, Tokyo 108-8639, Japan

⁴ Department of Pathology, Kyorin University, School of Medicine, 6-20-2, Shinkawa, Mitaka-shi, Tokyo 181-0004, Japan

⁵ Department of Pathology, Graduate School of Medicine, The University of Tokyo, 7-3-1, Hongo, Bunkyo-ku, Tokyo 113-0033, Japan

⁶ International University of Health and Welfare, 2600-1 kitakanamaru, Otawara, Tochigi 324-8501, Japan

⁷ Department of Radiology, International University of Health and Welfare Hospital, 537-3, Iguchi, Nasushiobara, Tochigi 329-2763, Japan

Abbreviations

ALB	Albumin
ALT	Alanine aminotransferase
AST	Aspartate aminotransferase
AUC	Area under the ROC curve
INR	International normalized ratio
NAFLD	Nonalcoholic fatty liver disease
NAS	NAFLD activity score
NASH	Nonalcoholic steatohepatitis
NECT	Non-contrast-enhanced computed tomography
PT	Prothrombin time
ROC	Receiver operating characteristic
ROI	Region of interest
SD	Standard deviation
SSF	Spatial scaling factors
T-Bil	Total bilirubin

Introduction

Nonalcoholic fatty liver disease (NAFLD) is a common condition worldwide, with a prevalence in the US of 19% [1]. Within the NAFLD spectrum, non-alcoholic steatohepatitis (NASH) causes severe liver diseases including advanced fibrosis, hepatic failure, and hepatocellular carcinoma [2]. Ultrasound-guided liver biopsy is the gold standard diagnostic test for NASH, but screening biopsies are discouraged as they are costly and invasive [3]. Thus, it is important that a method is developed for the noninvasive identification of patients who are at high risk of NASH, and in whom a biopsy as part of further diagnostic work-up is warranted.

Previous research has shown that several serum markers are elevated in patients with NASH compared with their levels in controls. Elevated markers include alanine aminotransferase (ALT) [4, 5], gamma glutamyl-transferase [5], and cytokeratin-18 [6]. However, other studies have shown a lack of an apparent threshold for serum ALT [7] and low diagnostic sensitivity for serum cytokeratin-18 in patients with NASH [8].

Regarding imaging techniques, some studies have demonstrated a correlation between steatosis grade obtained using abdominal ultrasonography and the risk of NASH [4, 5]. In addition, several groups have used computed tomography (CT) texture analysis to aid in the staging of hepatic fibrosis [9–11] as related to the progression of NASH. However, despite the routine availability of non-contrast-enhanced CT (NECT), no study has yet sought to diagnose NASH using this modality.

Texture analysis quantifies regional heterogeneity [12, 13], which is a recognized feature of malignant tumour biology [14]. In texture analysis, regional heterogeneity is represented by texture parameters calculated based on a variety of mathematical methods to evaluate the grey-level intensity of a pixel

and its position within an image [12, 14]. The most common method is to quantify statistical values from the grey-level frequency distribution within the region of interest (ROI), which can be obtained from the histogram of pixel intensities. Recently, texture analysis has been applied to the assessment of several pathologies, including tumours [15–18].

We hypothesized that CT texture analysis could be used to identify patients at high risk of NASH. As pre-existing liver fibrosis can affect CT texture features [19], we chose to group patients based on the biochemical suspicion of pre-existing fibrosis. CT texture and its relationship to NASH were assessed separately in these groups. Our purpose was to explore whether CT texture analysis could be used to predict the presence of NASH accurately.

Materials and methods

This study was approved by the Research Ethics Committee as a retrospective data analysis for medical imaging-based diagnoses (2561-12). The committee waived the requirement for informed consent.

Patients

Initially, a total of 143 patients who underwent a liver biopsy at our institution between August 2006 and April 2016 for the diagnosis of suspected NASH were recruited for this study. Patients who used alcohol (>30 g/day in men and >20 g/day in women) were excluded. A total of 88 patients (average age 64.5 ± 12.0 years, 50 men and 38 women) with suspected NASH based on abnormal liver function test results underwent both abdominal NECT and liver biopsy during this period. The mean interval between NECT and liver biopsy was 2.9 months. All relevant laboratory data were obtained from the patient electronic medical records, including the levels of serum albumin (ALB), aspartate aminotransferase (AST), ALT, serum hyaluronic acid, total bilirubin (T-Bil), prothrombin time (PT), and the international normalized ratio (INR). Histories of alcohol intake were obtained from a database of liver biopsies maintained by the Department of Gastroenterology and Hepatology.

CT image acquisition

CT was performed using a 320-detector row scanner (Aquilion One; Toshiba Medical Systems Corp., 11 patients) or various 64-detector row scanners (Aquilion Prime in 11 patients, Aquilion 64 scanner in 34 patients, both Toshiba Medical Systems; Discovery CT750 HD in 27 patients, LightSpeed VCT in 5 patients, both GE Medical Systems). All scanners used the identical clinical protocol: 120 kV, 100–450 mA (depending on the anatomical location;

automatic exposure control systems were employed), 0.5 s per rotation, pitch 0.8–1.4:1, matrix 512, thickness 5 mm, and field-of-view 400–500 mm. For image reconstruction, filtered back-projection was used with a soft-tissue kernel (FC03 in 25 patients, FC04 in 31 patients) with the Aquilion One, Aquilion Prime and Aquilion 64 scanners; or a standard kernel in 32 patients with the Discovery CT750 HD and LightSpeed VCT scanners). Five NECT examinations were performed as noncontrast studies alone and 83 NECT examinations were combined with contrast-enhanced CT.

Texture analysis

A single image slice from the level of the umbilical portion of the portal vein was loaded into the workstation for texture analysis. The TexRAD (TexRAD Ltd.) proprietary research algorithm was used to quantify the textural properties of each image. A circular ROI 2 cm in diameter was placed in the right

anterior segment of the liver by the operator, a board-certified radiologist with 5 years' experience with abdominal CT in conjunction with a board-certified radiologist with 23 years' experience of abdominal CT. The diameter was chosen so as to maximize the size of the ROI while excluding intrahepatic vessels. The right anterior segment was chosen as it is typically the location selected for biopsy, and avoids potential artefacts caused by the vertebral bodies and the heart.

Texture assessment involved an initial filtration step. A Laplacian of Gaussian spatial band-pass filter was used for the selective extraction of features of differing size and intensity with three spatial scaling factors (SSF): fine (feature width about 1 mm), medium (feature width about 2 mm), and coarse (feature width about 4 mm; Fig. 1). Filtration was applied to reduce CT photon noise, which may affect texture assessment [14]. The SSF was noted following the analyzed parameters. For example, the calculated mean in unfiltered images was recorded as mean0 and the calculated entropy in filtered

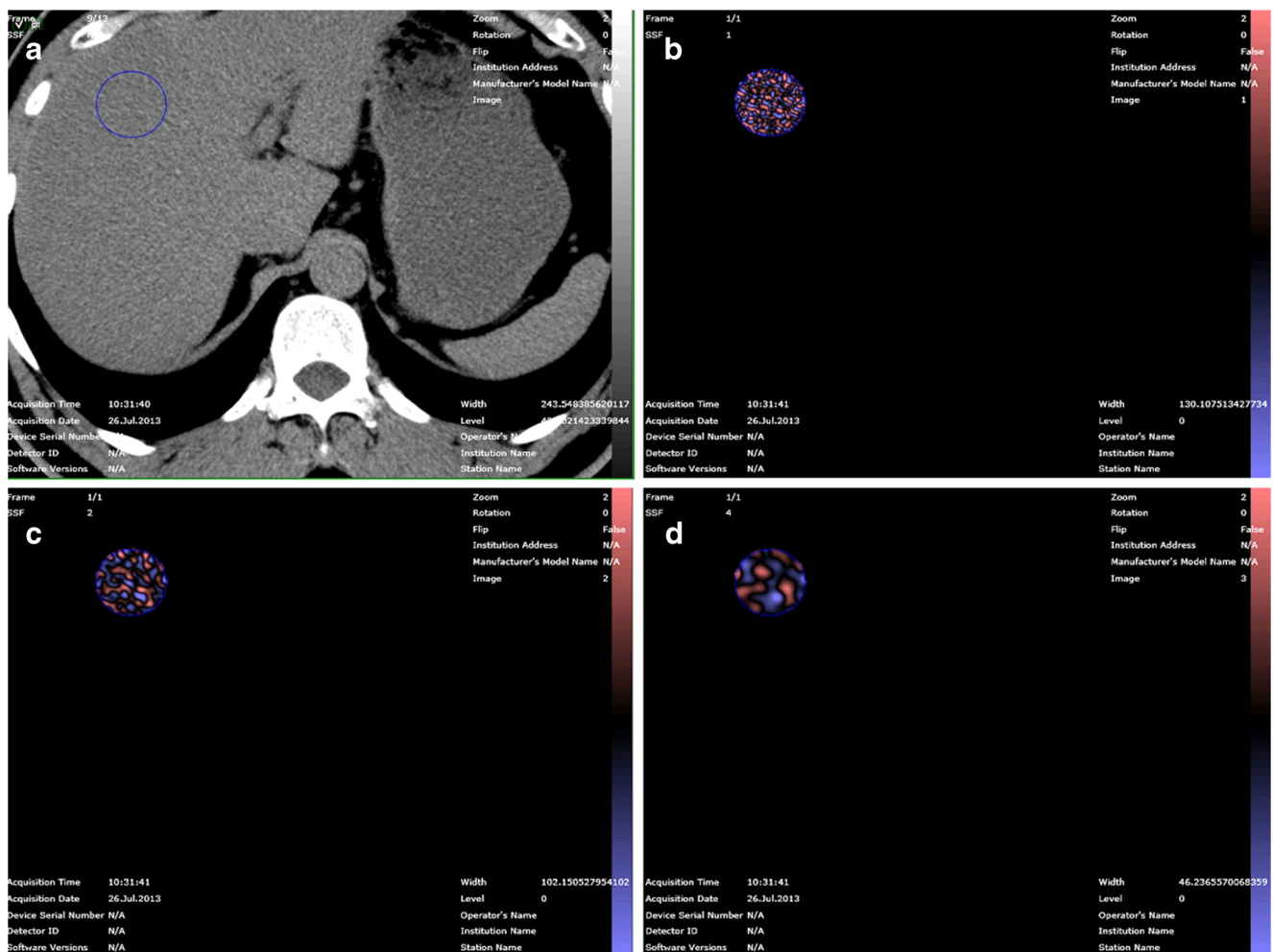


Fig. 1 Texture analysis of CT images of the liver. **a** A non-contrast-enhanced CT image in a 57-year-old man shows a region of interest in the right anterior lobe. **a–c** The corresponding postprocessed CT images reveal **(b)** fine, **(c)** medium and **(d)** coarse textures obtained with fine (1

mm), medium (2 mm) and coarse (4 mm) filtration, respectively. The images are displayed using a red–blue scale indicating negative–positive pixels respectively.

images with an SSF of 4 mm was recorded as entropy. Heterogeneity was obtained by analysis of the ROI histogram and each feature of heterogeneity was set as a parameter according to previous studies [12, 14]. The average grey-level intensity of pixels inside the ROI and the variation from the mean intensity were set as parameter mean and standard deviation, respectively (Fig. 2). The average intensity of the positive grey-level signals from pixels within the ROI was set as parameter mean of positive pixels (Fig 3). Asymmetry and pointedness of the distribution were set as parameters skewness and kurtosis, respectively (Figs. 4 and 5). The irregularity or complexity of the grey-level intensity was set as parameter entropy. Generally, a lower entropy represents a more regular (i.e. homogeneous) distribution and a higher entropy represents a more irregular/complex (i.e. heterogeneous) distribution.

Liver biopsy and pathology

A percutaneous 16-gauge needle core biopsy of the right hepatic lobe was performed using ultrasound by a hepatologist blinded to the clinical data and study design. The Department of Pathology processed all specimens. Biopsy reports were prepared using the NASH Clinical Research Network histological scoring scheme [20]. This score incorporates both the NAFLD Activity Score (NAS; grades 0–8) and fibrosis stage (grades 0, 1a, 1b, 1c, 2, 3 and 4). The NAS is the sum of the steatosis score (0–3), the lobular inflammation score (0–3), and the hepatocyte ballooning score (0/2).

Statistical analysis

Patients were divided into two groups in ascending order of the date of liver biopsy to form a learning dataset comprising 53 patients (60%) and a validation dataset comprising 35 patients (40%). As fibrosis influences CT texture [19], the patients were further subdivided based on the suspicion of pre-

existing fibrosis (Fig. 6). A serum hyaluronic acid cut-off level of 50 $\mu\text{g/L}$ was used to predict fibrosis grades 3 and 4 [21].

The learning dataset group with and without suspicion of fibrosis was used to select appropriate variables and to create a multiple logistic regression model that predicted the presence or absence of NASH. NASH was considered present when the NAS was ≥ 3 , as scores of 0 and 2 are not diagnostic of steatohepatitis [20]. First, we constructed receiver operating characteristic (ROC) curves to assess which parameters derived from texture analysis best predicted $\text{NAS} \geq 3$, and the areas under the ROC curves (AUCs) of each parameter were measured, including the mean, standard deviation, entropy, mean of positive pixels, skewness, and kurtosis. Parameters with AUCs > 0.65 were then subjected to stepwise regression analysis including bidirectional elimination (inclusion and exclusion thresholds, 0.25) to create a multiple logistic model predictive of NASH. The cut-off value was selected according to the Youden index (the highest sum of sensitivity plus specificity minus one). Finally, the multiple logistic model and the defined cut-off values were applied to the validation dataset, and diagnostic performance, including accuracy, sensitivity, specificity, and positive and negative predictive values, was calculated.

The patients' background characteristics including age, ALT, AST, serum hyaluronic acid, ALB, T-Bil, PT-INR and NAS were compared using a *t* test, and Child–Pugh class, ascites grade, steatosis scores, lobular inflammation status, hepatocyte ballooning and fibrosis stage were compared using the chi-squared test between patients with and without suspicion of fibrosis. All statistical analyses were performed with JMP 11.2.0 (SAS Inc., Cary, NC). All data are presented as means \pm standard deviation.

Results

Patient data grouped by serum hyaluronic acid status are shown in Table 1. Patients with elevated serum hyaluronic acid levels had significantly higher age, Child–Pugh scores,

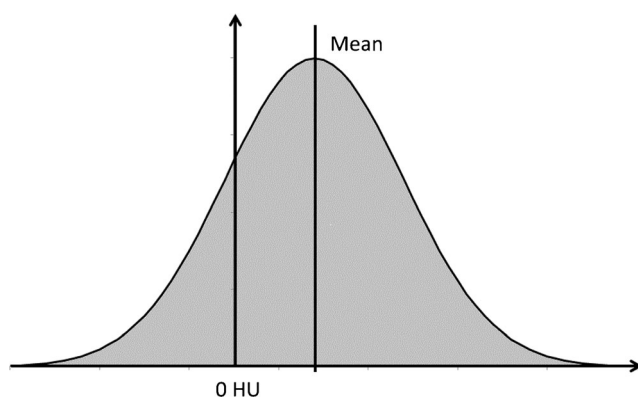


Fig. 2 Illustration of the parameter 'mean' (the simple average of all the pixel values)

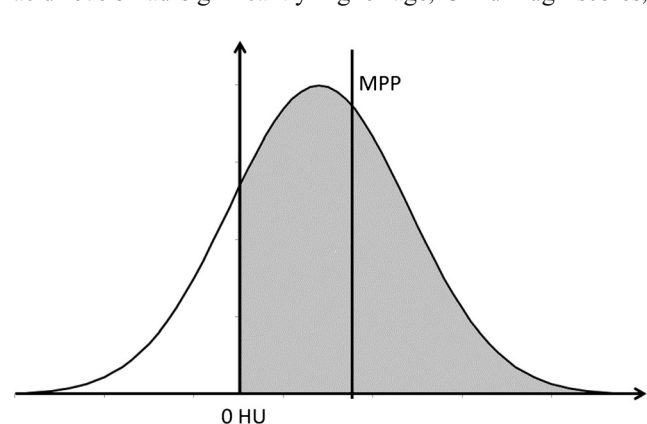
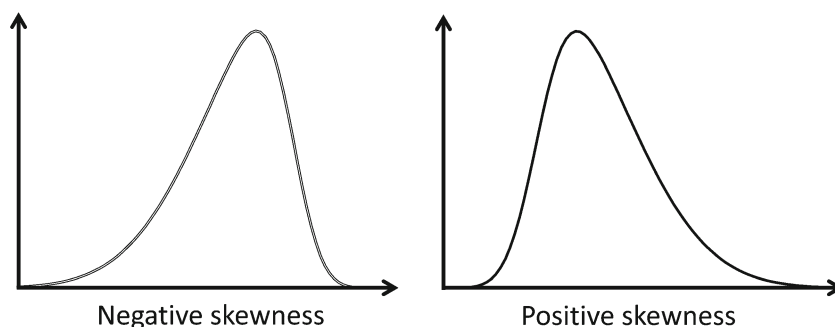


Fig. 3 Illustration of the mean positive pixel value (MPP)

Fig. 4 Illustration of positive and negative skewness. The parameter ‘skewness’ represents the degree and direction of asymmetry



T-Bil levels, PT-INR, pathological steatosis scores, and fibrosis stage. In addition, patients with elevated serum hyaluronic acid levels had significantly lower ALT and ALB. Of the 36 patients without elevated levels of serum hyaluronic acid (<50 µg/L), 28 (77.8%) had fibrosis stages 0–2. Of the 52 patients with elevated serum hyaluronic acid levels (≥50 µg/L), 45 (86.5%) had fibrosis stage 3 or 4. A cut-off value of 50 µg/L was effective in predicting the presence or absence of liver fibrosis in 83% of patients (73/88). The NAS scores did not differ significantly between the two groups.

Table 2 shows the AUCs of the texture parameters predicting NAS ≥3, derived from ROC analysis of the learning dataset. There were 12 parameters with AUCs >0.65 in patients without elevated serum hyaluronic acid levels. Mean0 and skewness2 remained after stepwise regression analysis, and a multiple logistic model with these parameters was used for prediction of NASH in this group. The cut-off value obtained was 0.45:

$$\ln(p/(1-p)) = -12.4 + 0.27 \times \text{mean0} + 4.06 \times \text{skewness2}$$

When the predictive model was applied to the learning and validation datasets, the AUC values were 0.93 and 0.94, respectively. The diagnostic performance values of the

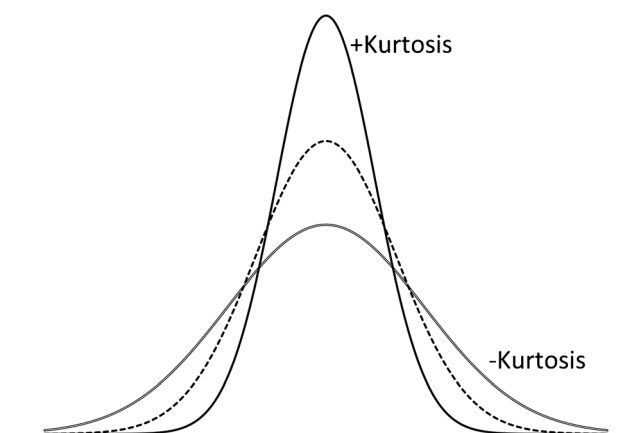


Fig. 5 Illustration of positive and negative kurtosis. The parameter ‘kurtosis’ represents the extent of the distribution’s tail (single line positive kurtosis, double line negative kurtosis, dashed line normal distribution)

predictive model using the cut-off value obtained were: accuracy 94%, specificity 92%, sensitivity 100%, positive predictive value 100%, and negative predictive value 80%.

In the learning dataset patients with elevated levels of serum hyaluronic acid, only mean0 and kurtosis4 had AUCs >0.65. Both parameters remained following stepwise regression analysis. A multiple logistic model using these two parameters was used for prediction of NASH in this group. The cut-off value obtained was 0.81:

$$\ln(p/(1-p)) = -10.18 + 0.18 \times \text{mean0} + 0.69 \times \text{kurtosis4}$$

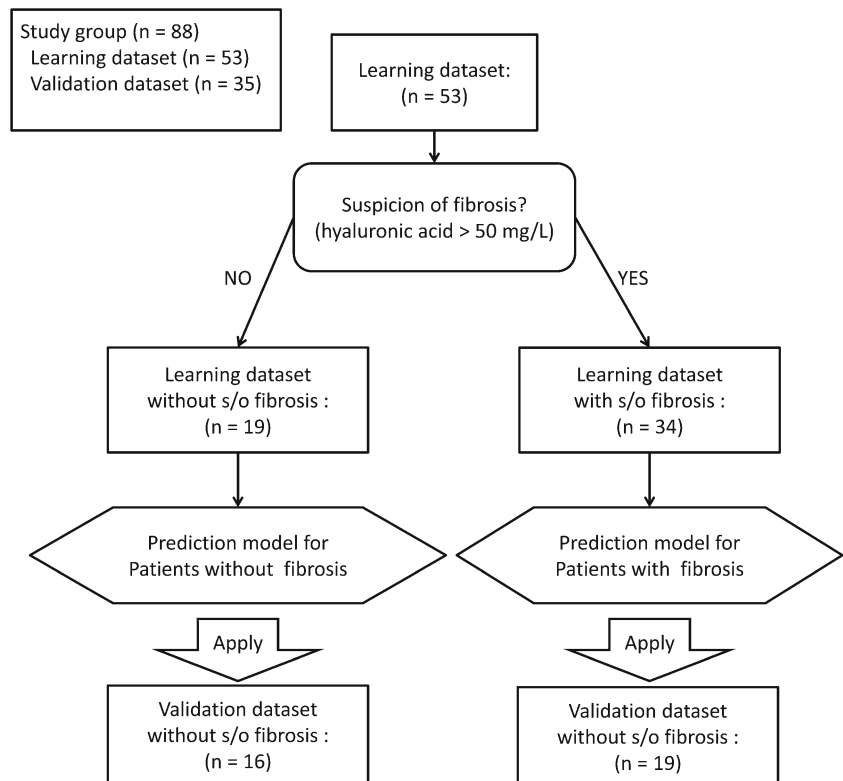
When the predictive model was applied to the learning and validation datasets, the AUC values were 0.81 and 0.60, respectively. The diagnostic performance values of the predictive model with the cut-off value obtained were: accuracy 42%, specificity 31%, sensitivity 100%, positive predictive value 100%, and negative predictive value 21%.

Discussion

This is the first study to show that NECT texture features can predict the risk of NASH. As discussed above, NAS ≥3 indicates the strong possibility of steatohepatitis and NASH. In patients without elevated levels of serum hyaluronic acid, mean0 and skewness2 were modest predictors of NAS ≥3. A predictive model using these two parameters predicted NASH with an accuracy of 92% in the validation dataset. In patients with suspected liver fibrosis as indicated by elevated levels of serum hyaluronic acid, mean0 and kurtosis4 were modest predictors of NAS ≥3. In this group, a predictive model using these two parameters predicted NASH in the validation dataset with only 42% accuracy. Although CT is widely used to screen for hepatocellular carcinoma in patients with a fatty liver, CT has not been used to diagnose NASH [2]. We found that NECT texture features accurately predicted a higher NAS in patients without elevated serum hyaluronic acid levels.

A recent study found that multiparametric assessment using MRI can distinguish NASH from simple steatosis

Fig. 6 Patient flow diagram (s/o suspicion of)



[22]. However, MRI signal values and acquisition protocols vary, and between-hospital results may be more variable than those found using CT, with which absolute tissue densities are calculated in Hounsfield units. Furthermore, MRI is more expensive and less accessible than CT. We used NECT data in the present study because NECT is essential for the diagnosis of fatty liver, and texture features of contrast-enhanced CT images are influenced by both the acquisition protocol and haemodynamic factors. Dynamic contrast-enhanced CT is recommended for all patients with a diagnosis of NASH but not for all patients with suspected NASH. Whatever the indication, NECT is commonly available and could also be used to provide information for texture analysis without the need for additional imaging.

The unfiltered means are the CT attenuations. Low-level attenuation reflects both macroscopic fat and fat-containing lesions with various proportions of fat and water [23]. NASH is pathologically characterized by steatosis, inflammation and hepatocellular ballooning. Both steatosis and inflammation reduce liver attenuation. The accumulations of fat and water induced by inflammation are less dense than normal hepatic parenchyma. Therefore, it is expected that low-level CT attenuation accompanies NASH. We found that skewness2 also contributed to NASH prediction. Skewness reflects asymmetry of the pixel histogram of the ROI [14]. This may be related to an unusual distribution of hepatic tissue in patients with NASH.

In patients with suspected fibrosis, defined as a serum hyaluronic acid level $>50 \mu\text{g/L}$, texture features did not accurately predict $\text{NAS} \geq 3$. Liver CT texture features are modified by fibrosis [9–11], and fibrosis may mask the texture features of NASH. It is therefore difficult to predict NASH in patients with advanced liver fibrosis. In such patients, an alternative noninvasive imaging method is required.

We performed first-order texture analysis by constructing histograms. Some reports have indicated that higher-order texture analysis is helpful in the diagnosis of liver metastasis [24], prostate cancer [25] and glioblastoma [26]. Histogram analysis is simpler and more practical, and should soon be routinely available on DICOM viewers.

We used elevated serum hyaluronic acid levels to predict liver fibrosis of stages 3 and 4. Previous studies have shown that a cut-off value of $42.0 \mu\text{g/L}$ has high sensitivity and specificity (100% and 89%, respectively) [27], as does a cut-off value of $46.1 \mu\text{g/L}$ (85% and 80%, respectively) [21]. In our study, a serum hyaluronic acid cut-off value of $50 \mu\text{g/L}$ was effective in predicting the presence or absence of liver fibrosis in 83% (73/88) of patients. A previous study has shown that fibrosis influences texture features in CT images of patients with varying extents of hepatic fibrosis [19]. In this study, we found that hepatic fibrosis masks the characteristic texture features of NASH, and that these features are more pronounced in patients without suspicion of pre-existing fibrosis.

Table 1 Patient data

	Normal hyaluronic acid level ($<50 \mu\text{g/L}$; $n = 35$)	Elevated hyaluronic acid level ($50 \geq \mu\text{g/L}$; $n = 53$)	<i>p</i> value
Gender (male/female)	24/11	26/27	0.07
Age (years)	55.9 ± 11.9	70.2 ± 7.3	<0.05
Liver enzyme levels (IU/L)			
ALT	71.1 ± 57.8	50.5 ± 22.5	<0.05
AST	44.1 ± 23.8	49.6 ± 34.0	0.20
Serum hyaluronic acid level (ng/mL)	24.2 ± 11.2	265.2 ± 287.1	<0.05
Child–Pugh A/B/C score, A/B/C	35/0/0	44/9/0	<0.05
Albumin (g/dL)	4.2 ± 0.3	3.7 ± 0.6	<0.05
Total bilirubin (mg/dL)	0.78 ± 0.31	1.1 ± 0.4	<0.06
Prothrombin time/international normalized ratio	1.03 ± 0.02	1.12 ± 0.14	<0.05
Ascites, yes/no	0/35	5/48	0.15
Pathology			
NAS (sum)	3.7 ± 1.8	3.1 ± 1.4	0.10
Steatosis, 0/1/2/3	2/16/11/6	10/37/5/1	<0.05
Lobular inflammation, 0/1/2/3	2/21/12/0	6/36/11/0	0.30
Hepatocyte ballooning, 0/1/2	14/15/6	10/30/13	0.09
Fibrosis stage, 0/1/1a/1b/1c/2/3/4	11/1/3/5/1/7/6/1	0/0/1/1/0/6/20/25	<0.05

The data presented are averages \pm standard deviations, or number of patients, as appropriate
NAS nonalcoholic fatty liver disease activity score

Table 2 AUCs of texture parameters for NASH prediction

Texture parameter	Filter level	Without suspicion of hepatic fibrosis			With suspicion of hepatic fibrosis		
		AUC	Youden index	Cut-off value	AUC	Youden index	Cut-off value
Mean	0	0.92 ^a	0.71	49.3	0.81 ^a	0.60	55.1
	1	0.70 ^a	0.44	−0.72	0.51	0.18	1.10
	2	0.70 ^a	0.46	−0.26	0.47	0.099	0.96
	4	0.70 ^a	0.61	0.00	0.53	0.21	2.80
Standard deviation	0	0.60	0.33	15.9	0.63	0.30	10.7
	1	0.68 ^a	0.44	41.3	0.49	0.17	31.6
	2	0.69 ^a	0.46	19.0	0.50	0.10	17.8
	4	0.39	0.14	10.4	0.53	0.20	9.33
Entropy	0	0.59	0.33	4.05	0.62	0.28	3.90
	1	0.66 ^a	0.35	4.64	0.50	0.24	4.81
	2	0.68 ^a	0.38	4.19	0.47	0.15	4.10
	4	0.67 ^a	0.40	3.36	0.54	0.29	3.52
Mean of positive pixels	0	0.92 ^a	0.71	49.3	0.81	0.60	55.1
	1	0.64	0.44	32.1	0.53	0.19	34.1
	2	0.61	0.29	11.3	0.51	0.15	15.2
	4	0.54	0.25	4.30	0.58	0.29	8.66
Skewness	0	0.64	0.38	0.01	0.58	0.35	0.13
	1	0.71 ^a	0.52	−0.02	0.59	0.42	0.12
	2	0.71 ^a	0.55	0.03	0.58	0.20	0.040
	4	0.51	0.35	−0.30	0.50	0.23	−0.30
Kurtosis	0	0.61	0.32	−0.18	0.52	0.21	0.01
	1	0.61	0.36	0.010	0.61	0.35	0.16
	2	0.63	0.35	−0.030	0.54	0.21	0.12
	4	0.64	0.30	−0.49	0.69 ^a	0.42	0.17

^a AUC >0.65

Our study had several limitations. First, several different CT scanners were used. The scan parameters were controlled in a single institution and interscanner differences in radiomic features were known [28]. In addition, filtration was used, which reduces the effect of photon noise when assessing texture features [28] and may have decreased interscanner differences. Second, the study population was small. This was because the indications for liver biopsy in patients with suspected NASH are limited. NASH is typically diagnosed by excluding other possible causes of hepatic impairment such as alcohol consumption, hepatitis B or C virus infection, and drug-induced hepatitis. However, pathological data were available for all patients, and our new noninvasive diagnostic method was useful when selecting patients for liver biopsy.

Third, despite avoiding visible hepatic vessels by manually creating ROIs in the anterior right lobe of the liver, it is possible that some ROIs may have contained some portion of a vessel. It can be difficult to identify vessels in a fatty liver because the vessels and the liver parenchyma are of similar density. However, the vessel area in the peripheral zone of the liver is small. Fourth, we used a single slice for texture analysis in this study. In some reported studies, three-dimensional ROIs have been used for texture analysis, particularly when performing assessments for neoplasm [29–31]. The heterogeneity inside the tumour is thought to be associated with variations in genomic subtype, gene expression, angiogenic factors, and the tumour microenvironment [32]. These variations depend on the location in the tumour and a three-dimensional analysis reveals texture features in the whole lesion. The liver in NASH may show less location-dependent variance than tumours. Therefore, we believe that the texture features were sufficiently demonstrated using a single-slice, two-dimensional assessment.

Fifth, radiation exposure is an inevitable issue in CT. Ultrasonography is a simple and noninvasive examination; however, the procedure depends on the skill of the operator, patient body habitus, and overlying bowel gas. MRI can provide reproducible images without radiation exposure, but CT is less expensive and more accessible than MRI, as discussed above. Therefore, we believe that it is meaningful to establish the assessment of NASH using CT. Finally, as our population consisted of only patients with the suspicion of NASH from their clinical information, it initially had a high pretest probability of NASH, which was considered to have contributed to the high sensitivity of the results.

Our study results might be useful in assessment before liver biopsy, allowing an unnecessary, invasive procedure to be avoided. To confirm the applicability of our results for distinguishing patients with NASH from the more general population, further cohort studies including more patients without suspicion of NASH are required.

Conclusions

In conclusion, texture analysis of NECT images allowed prediction of the presence of NASH with an accuracy of 92% in patients without fibrosis. In patients with elevated hyaluronic acid levels, associated with the presence of fibrosis, no model provided accurate prediction.

Funding We received no financial support for this study.

Compliance with ethical standards

Guarantor The scientific guarantor of this publication is Shigeru Kiryu.

Conflict of interest The authors of this manuscript declare no relationships with any companies, whose products or services may be related to the subject matter of the article.

Statistics and biometry Authors S.N. and S.K. have significant statistical expertise.

Informed consent The need for written informed consent was waived by the Institutional Review Board.

Ethical approval Institutional Review Board approval was obtained.

Methodology

- retrospective
- diagnostic study
- performed at one institution

References

1. Lazo M, Hernaez R, Eberhardt MS et al (2013) Prevalence of non-alcoholic fatty liver disease in the United States: The Third National Health and Nutrition Examination Survey, 1988–1994. *Am J Epidemiol* 178:38–45
2. Goh GB-B, McCullough AJ (2016) Natural history of nonalcoholic fatty liver disease. *Dig Dis Sci* 61:1226–1233
3. Chalasani N, Younossi Z, Lavine JE et al (2012) The diagnosis and management of non-alcoholic fatty liver disease: Practice Guideline by the American Association for the Study of Liver Diseases, American College of Gastroenterology, and the American Gastroenterological Association. *Hepatology* 55:2005–2023
4. Salman AAA, Aboelfadl SAE, Heagzy MAE (2016) New era for usage of serum liver enzymes as a promising horizon for the prediction of non-alcoholic fatty liver disease. *Open Access Maced J Med Sci* 4:348–352
5. Pulzi FB, Cisternas R, Melo MR et al (2011) New clinical score to diagnose nonalcoholic steatohepatitis in obese patients. *Diabetol Metab Syndr* 3:3
6. Kwok R, Tse Y-K, Wong GL-H et al (2014) Systematic review with meta-analysis: non-invasive assessment of non-alcoholic fatty liver disease – the role of transient elastography and plasma cytochrome-k18 fragments. *Aliment Pharmacol Ther* 39:254–269
7. Verma S, Jensen D, Hart J, Mohanty SR (2013) Predictive value of ALT levels for non-alcoholic steatohepatitis (NASH) and advanced fibrosis in non-alcoholic fatty liver disease (NAFLD). *Liver Int* 33: 1398–1405

8. Cusi K, Chang Z, Harrison S et al (2014) Limited value of plasma cytokeratin-18 as a biomarker for NASH and fibrosis in patients with non-alcoholic fatty liver disease. *J Hepatol* 60:167–174
9. Dagnawala N, Li B, Buch K et al (2016) Using texture analyses of contrast enhanced CT to assess hepatic fibrosis. *Eur J Radiol* 85: 511–517
10. Zhang X, Gao X, Liu BJ et al (2015) Effective staging of fibrosis by the selected texture features of liver: Which one is better, CT or MR imaging? *Comput Med Imaging Graph* 46:227–236
11. Kayaaltı Ö, Aksebzeci BH, Karahan İÖ et al (2014) Liver fibrosis staging using CT image texture analysis and soft computing. *Appl Soft Comput* 25:399–413
12. Davnall F, Yip CSP, Ljungqvist G et al (2012) Assessment of tumor heterogeneity: an emerging imaging tool for clinical practice? *Insights Imaging* 3:573–589
13. Raman SP, Schroeder JL, Huang P et al (2015) Preliminary data using computed tomography texture analysis for the classification of hypervascular liver lesions. *J Comput Assist Tomogr* 39: 383–395
14. Ganeshan B, Miles KA (2013) Quantifying tumour heterogeneity with CT. *Cancer Imaging* 13:140–149
15. Kassner A, Thornhill RE (2010) Texture analysis: a review of neurologic MR imaging applications. *AJNR Am J Neuroradiol* 31: 809–816
16. Kiryu S, Akai H, Nojima M et al (2017) Impact of hepatocellular carcinoma heterogeneity on computed tomography as a prognostic indicator. *Sci Rep* 7:12689
17. Yasaka K, Akai H, Nojima M et al (2017) Quantitative computed tomography texture analysis for estimating histological subtypes of thymic epithelial tumors. *Eur J Radiol* 92:84–92
18. Ganeshan B, Abaleke S, Young RCD et al (2010) Texture analysis of non-small cell lung cancer on unenhanced computed tomography: initial evidence for a relationship with tumour glucose metabolism and stage. *Cancer Imaging* 10:137–143
19. Wu Z, Matsui O, Kitao A et al (2015) Hepatitis C related chronic liver cirrhosis: feasibility of texture analysis of MR images for classification of fibrosis stage and necroinflammatory activity grade. *PLoS One* 10:e0118297
20. Kleiner DE, Brunt EM, Van Natta M et al (2005) Design and validation of a histological scoring system for nonalcoholic fatty liver disease. *Hepatology* 41:1313–1321
21. Suzuki A, Angulo P, Lymp J et al (2005) Hyaluronic acid, an accurate serum marker for severe hepatic fibrosis in patients with non-alcoholic fatty liver disease. *Liver Int* 25:779–786
22. Pavlides M, Banerjee R, Tunnicliffe EM et al (2017) Multiparametric magnetic resonance imaging for the assessment of non-alcoholic fatty liver disease severity. *Liver Int* 37:1065–1073
23. Valls C, Iannaccone R, Alba E et al (2006) Fat in the liver: diagnosis and characterization. *Eur Radiol* 16:2292–2308
24. Ahn SJ, Kim JH, Park SJ, Han JK (2016) Prediction of the therapeutic response after FOLFOX and FOLFIRI treatment for patients with liver metastasis from colorectal cancer using computerized CT texture analysis. *Eur J Radiol* 85:1867–1874
25. Nketiah G, Elschot M, Kim E et al (2017) T2-weighted MRI-derived textural features reflect prostate cancer aggressiveness: preliminary results. *Eur Radiol* 27:3050–3059
26. Molina D, Pérez-Beteta J, Luque B et al (2016) Tumour heterogeneity in glioblastoma assessed by MRI texture analysis: a potential marker of survival. *Br J Radiol* 89:20160242
27. Kaneda H, Hashimoto E, Yatsuji S et al (2006) Hyaluronic acid levels can predict severe fibrosis and platelet counts can predict cirrhosis in patients with nonalcoholic fatty liver disease. *J Gastroenterol Hepatol* 21:1459–1465
28. Mackin D, Fave X, Zhang L et al (2015) Measuring computed tomography scanner variability of radiomics features. *Investig Radiol* 50:757–765
29. Mahmoud-Ghoneim D, Toussaint G, Constans JM, De Certaines JD (2003) Three dimensional texture analysis in MRI: a preliminary evaluation in gliomas. *Magn Reson Imaging* 21:983–987
30. Park HJ, Kim JH, Choi SY et al (2017) Prediction of therapeutic response of hepatocellular carcinoma to transcatheter arterial chemoembolization based on pretherapeutic dynamic CT and textural findings. *AJR Am J Roentgenol* 209:W211–W220
31. Chen W, Giger ML, Li H et al (2007) Volumetric texture analysis of breast lesions on contrast-enhanced magnetic resonance images. *Magn Reson Med* 58:562–571
32. Nelson DA, Tan TT, Rabson AB et al (2004) Hypoxia and defective apoptosis drive genomic instability and tumorigenesis. *Genes Dev* 18:2095–2107